Structural Engineering and Mechanics, Vol. 19, No. 6 (2005) 603-618
DOI: http://dx.doi.org/10.12989/sem.2005.19.6.603

Adaptation of impactor for the split Hopkinson pressure bar in characterizing concrete at medium strain rate

Pengjun Zhao†

Centre for Protective Technology, National University of Singapore, Department of Civil Engineering, 10 Kent Ridge Crescent, Singapore 119260

Tat-Seng Lok‡

School of Civil and Environmental Engineering, Nanyang Technological University, Block N1, Nanyang Avenue, Singapore 639798

(Received March 18, 2004, Accepted January 24, 2005)

Abstract. The split Hopkinson pressure bar (SHPB) technique is widely used to characterize the dynamic mechanical response of engineering materials at high strain rates. In this paper, attendant problems associated with testing 70 mm diameter concrete specimens are considered, analysed and resolved. An adaptation of a conventional solid circular striker bar, as a means of achieving reliable and repeatable SHPB tests, is then proposed. In the analysis, a pseudo one-dimensional model is used to analyse wave propagation in a non-uniform striker bar. The stress history of the incident wave is then obtained by using the finite difference method. Comparison was made between incident waves determined from the simplified model, finite element solution and experimental data. The results show that the simplified method is adequate for designing striker bar shapes to overcome difficulties commonly encountered in SHPB tests. Using two specifically designed striker bars, tests were conducted on 70 mm diameter steel fibre reinforced concrete specimens. The results are presented in the paper.

Key words: split Hopkinson pressure bar; dynamic characteristics of concrete; strain rate effect; finite difference method; impact.

1. Introduction

Engineers may be asked to design special structures or facilities to withstand unusual loading histories such as resisting high-intensity, short duration loading. This time-dependant loading could arise from seismic shock activity or from exposure to air blast. In such circumstances, it is essential that engineers are aware of the nature of material behaviour at high strain rate. This is important because materials respond differently at quasi-static loading rate and at high loading rates. Understanding the dynamic properties of conventional building materials such as concrete, rock and steel is essential in the safe design and construction of facilities that may be subjected to short-

† Research Fellow
‡Associate Professor, Corresponding author, E-mail: CTSLOK@ntu.edu.sg

duration loading. To do this, specialised equipment is necessary to determine the behaviour of these materials.

The split Hopkinson pressure bar, or SHPB, (Kolsky 1949) has long been the main experimental equipment for testing metal specimens at strain rates from 10^1 to 10^3 per second. In such tests, a small circular solid disk, often about 5-10 mm in diameter and 2-3 mm in length, is sandwiched between two elastic pressure bars and loaded by a stress wave. By measuring the strain-time history in the pressure bars, the stress, strain and strain rate histories of the specimen can be determined. The SHPB technique can also be used to characterize the dynamic mechanical behaviour of heterogeneous materials such as rock and concrete (Tedesco and Ross 1989, Ross *et al.* 1989). However, a large specimen that contains a sufficient number of material components is needed to obtain representative results for concrete. This technique demands a correspondingly larger diameter split Hopkinson pressure bar.

Unfortunately, problems arise with the use of large diameter bars. These are:

- stress and strain uniformity in the specimen – this is more critical in large heterogeneous specimens than in small metal specimen.
- notion of one-dimensional wave theory – accurate in small diameter bars but is less accurate if large diameter bars are used; elastic wave propagating in a large pressure bar tends to be dispersive, resulting in strain difference from the centre to the surface of the pressure bar.
- wave shape change – occurs during propagation in dispersive wave. These causes inaccuracy in test results if data were processed by normal procedures.

The validity of SHPB test has been studied by many researchers in the past. Bertholf and Karnes (1975) conducted a two-dimensional numerical study on the typical SHPB set-up and concluded that SHPB test results are reliable if interface friction, specimen geometry and strain rate are within appropriate ranges. Meng and Li (2003) completed finite element simulation of SHPB tests based on a fine mesh and related the testing accuracy to the stress uniformity in the specimen. These studies are relevant to testing of metal specimens. Donze *et al.* (1999) conducted discrete particle analysis whose results indicated that the strength increase of a concrete specimen observed in SHPB tests is mainly attributed to structural effect. The equivalent single-degree-of-freedom analysis by Johansson (1999) also reveals the significant influence of structural effect on SHPB tests of the large concrete specimens.

The purpose SHPB test of the concrete specimen is to obtain the mechanical behaviour of the whole specimen which often represents the minimum acceptable size of a material which can be confidently referred to as concrete. Further division of the specimen into small elements results in the difficulty that the element behaviour is not defined. Obviously, the element in the finite element mesh has a different constitutive behaviour from the whole specimen. Conventional FE analysis uses the element behaviour which is obtained by testing a large concrete specimen will not yield correct structural behaviour of the SHPB specimen.

In this paper, a different approach is adopted to study the validity of the SHPB test of concrete specimen and in conducting reliable tests. Stress uniformity in the specimen is examined by solving the stress-time histories at the two ends of a specimen for the simplified test condition – one-dimensional elastic wave propagation along the pressure bars and within the specimen. The result is used as a basic qualitative guideline to design SHPB tests and to select the proper incident wave. A pseudo-one-dimensional method is then proposed to design a tapered striker bar to generate the incident wave with prolonged rise duration. Using the new striker bar, the stress at two ends of the specimen is shown as uniform prior to reaching the peak stress. Finally, dynamic test results of steel

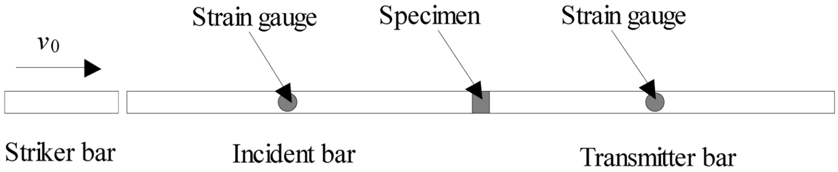

Fig. 1 Diagrammatic representation of a split Hopkinson pressure bar

fibre reinforced concrete (SFRC) specimens are presented to reinforce the hypothesis outlined in this paper.

2. Principles of SHPB and stress uniformity in specimen

The SHPB comprises a striker bar, an incident bar (input bar) and a transmitter bar (output bar) shown in Fig. 1. These bars are usually made from high strength steel, so that they remain elastic during the testing of high strength materials. A test specimen is sandwiched between the incident and transmitter bars. A striker bar is propelled by a gas gun and impacts the incident bar, resulting in an elastic compressive wave (incident wave) which propagates along the incident bar. As it reaches the specimen, a reflected wave and a transmitted wave (that continues into the transmitter bar) are generated. All three waves are recorded by two strain gauges fixed on the surface of the two long pressure bars.

The strain rate, strain and stress histories of the specimen can be determined from:

$$\dot{\varepsilon}(t) = \frac{c_0}{L_s}[\varepsilon_i(t) - \varepsilon_r(t) - \varepsilon_t(t)] \tag{1}$$

$$\varepsilon(t) = \frac{c_0}{L_s}\int_0^t [\varepsilon_i(t) - \varepsilon_r(t) - \varepsilon_t(t)]dt \tag{2}$$

$$\sigma(t) = \frac{AE}{2A_s}[\varepsilon_i(t) + \varepsilon_r(t) + \varepsilon_t(t)] \tag{3}$$

where $\varepsilon_i(t)$, $\varepsilon_r(t)$ and $\varepsilon_t(t)$ are the strain histories of the incident, reflected and transmitted waves respectively occurring at the incident bar/specimen interface and the specimen/transmitter bar interface; A_s and L_s are the cross-sectional area and length of the specimen respectively; A, E and c_0 are the cross-sectional area, Young's modulus and longitudinal wave velocity of the pressure bars respectively.

Eqs. (1)-(3) are valid provided that:

- the propagation of elastic waves through the pressure bars is described by one-dimensional wave theory – implying that small pressure bars are used to minimize wave dispersion; and
- uniform stress and strain distributions are attained within the specimen prior to failure.

The condition of one-dimensional elastic wave makes it possible to deduce strain-time histories at the interfaces from those recorded at the gauge locations, which are usually located at the mid-span of the two pressure bars. Also, the corresponding stress and velocity-time histories can be easily

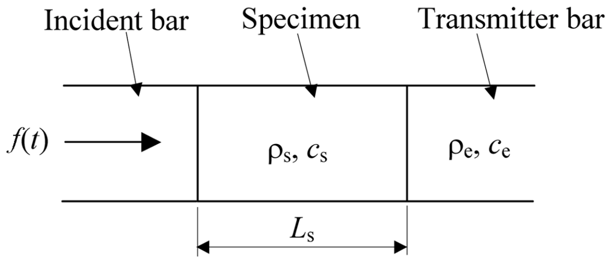

Fig. 2 One-dimensional model

calculated from the strain histories in one-dimensional wave condition. Interface friction imposes additional shear confinement on the specimen and radial inertia produces a distribution of radial stress. These two factors make the stress state in the specimen deviate from uni-axial compression. Further, longitudinal inertia causes non-uniform axial stress in the specimen and this makes the average stress (determined from the interface loads) deviate from the actual specimen stress.

Fortunately, interface friction can be reduced by applying a lubricant and wave dispersion can be corrected by a phase correction method in frequency domain (Follansbee and Frantz 1983). The longitudinal and radial inertia are all caused by dynamic effects associated with shock loading process and they are inter-related in that the radial inertia is weak when the longitudinal inertia is weak. Therefore, the most critical component is stress uniformity. This is because the measured stress and strain are meaningful only when the specimen is subjected to a nearly uniform stress state. Stress uniformity in the axial direction only is considered here. This is represented by the simplified one-dimensional model of the SHPB as shown in Fig. 2, in which the specimen is sandwiched between two elastic pressure bars.

Consider the incident wave propagating towards the specimen. Internally, the wave undergoes multiple reflection and transmission at the specimen/pressure bar interfaces. The wave transmitted by the incident bar/specimen interface produces compressive stress. The specimen is loaded when this compressive wave propagates through the specimen. Another compressive wave is generated because of reflection at the specimen/transmitter bar interface and this propagates back along the specimen. It further loads the specimen to a higher stress level. Similarly, another compressive wave will be reflected by the incident bar/specimen interface and this loads the specimen again. Clearly, the specimen is subjected to multiple internal reflections and stress uniformity is attained gradually with internal reflection.

The stress-time history at the incident bar/specimen interface can be obtained by superimposing the original incident wave and the subsequent reflected waves generated up to the current time. Similarly, the stress-time history at the specimen/transmitter bar interface can be obtained by superimposing all the transmitted waves present at the current time. Using one-dimensional elastic wave theory, the stress-time histories at the incident bar/specimen interface and the specimen/transmitter bar interface can be expressed, respectively, as:

$$\sigma_1(t) = (1+\lambda)f(t) + (1-\lambda^2)\sum_{i=1}^{[k/2]}(-\lambda)^{2i-1}f(t-2i\Delta) \tag{4}$$

$$\sigma_2(t) = (1-\lambda^2)\sum_{i=1}^{\left[\frac{k-1}{2}\right]+1}(-\lambda)^{2(i-1)}f[t-(2i-1)\Delta] \tag{5}$$

where

$$\lambda = \frac{\rho_s c_s - \rho_e c_e}{\rho_s c_s + \rho_e c_e} \tag{6}$$

$$k = \left[\frac{t}{\Delta}\right] \tag{7}$$

and in which ρ_s and c_s are the density and bar wave velocity of the specimen respectively; ρ_e and c_e are the same parameters of the pressure bar; Δ is the time interval needed for the stress wave to propagate through the length of the specimen; and $f(t)$ is the time history of the incident stress. Notation $[\cdot]$ denotes taking the maximum integer less than the number in the bracket.

The summation shown in Eqs. (4) and (5) is evaluated only if the upper limit is greater than or equal to the lower limit. These equations are applicable for any form of incident wave but the numerical result is evaluated here for a few special cases relevant to tests from an SHPB. For example, consider a rectangular incident wave. In this case, the incident stress σ_0 is a constant value at $t \geq 0$. Assuming a typical value of $\lambda = -0.6243$, the calculated result is summarised in Table 1. In this table, stress non-uniformity is expressed in terms of a relative stress difference defined as:

$$e_r = \frac{\sigma_2 - \sigma_1}{\sigma_1} \tag{8}$$

The relative error falls below 5% when $k \geq 6$, so that if a rectangular incident wave is used on the specimen, the specimen should fail after three rounds of internal reflection to achieve maximum 5% stress non-uniformity. The axial stress in the specimen at this time exceeds 91% of the incident stress. This means that the incident stress should be a little higher than the specimen strength. Therefore, only one incident stress can be used to test specimens for a rectangular incident wave. Stress uniformity in the specimen will be violated if there is an increase in the incident stress to achieve a higher strain rate.

To appreciate the significance of the rectangular incident wave, its rise-time should be compared

Table 1 Solution of rectangular incident wave

k	σ_1/σ_0	σ_2/σ_0	e_r
0	0.3575	0	–1
1	0.3575	0.6102	0.7069
2	0.7200	0.6102	–0.1525
3	0.7200	0.8365	0.1618
4	0.8613	0.8365	–0.0288
5	0.8613	0.9247	0.0737
6	0.9164	0.9247	0.0091
7	0.9164	0.9591	0.0466

with the time interval, Δ. For a concrete specimen, 35 mm in length and 70 mm in diameter, Δ is 8.75 μs for a typical wave velocity of 4000 m/s. The rise-time of a rectangular wave must be much shorter than 8.75 μs. This requirement is difficult to achieve for a large diameter SHPB. So, the rectangular wave is not appropriate in tests on large diameter concrete specimens.

Consider next a linearly increasing incident wave. The stress of such an incident wave can be written as:

$$f(t) = \dot{\sigma}t \tag{9}$$

where $\dot{\sigma}$ denotes the rate at which the incident stress rises.

Substituting Eq. (9) into Eqs. (4) and (5) leads to the following expressions for interface stresses:

$$\sigma_1(t) = (\dot{\sigma}\Delta)\mu\left[(1+\lambda) + (1-\lambda^2)\sum_{i=1}^{[k/2]}(-\lambda)^{2i-1}\frac{\mu-2i}{\mu}\right] \tag{10}$$

$$\sigma_2(t) = (\dot{\sigma}\Delta)\mu(1-\lambda^2)\sum_{i=1}^{\left[\frac{k-1}{2}\right]+1}(-\lambda)^{2(i-1)}\frac{\mu-(2i-1)}{\mu} \tag{11}$$

where μ is the normalized time expressed as:

$$\mu = \frac{t}{\Delta} \tag{12}$$

The relative stress difference obtained from Eqs. (10) and (11) is plotted in Fig. 3. Unlike the rectangular incident wave, the relative stress difference for the linear incident wave tends to zero monotonically with increase in time. The relative stress difference falls below 5% only after $\mu \geq 6.6$. At this time, the value of σ_1 reaches 0.71 times the incident stress.

Linear incident wave is representative of SHPB tests because in most cases the specimen fails at the rising edge of the incident wave. Clearly, the discussion above shows that the rise-time of the incident wave should be greater than 60 μs in testing concrete specimens. This cannot be satisfied if a conventional constant diameter circular striker bar is used; the incident wave generated by this striker produced a rise-time of ≤ 30 μs. Therefore, adapting the conventional striker bar is necessary to obtain reliable data when testing large diameter concrete specimens.

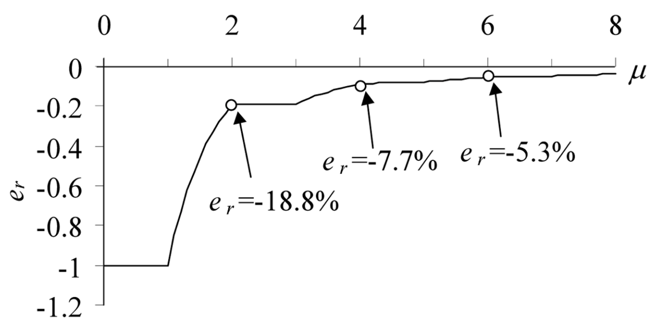

Fig. 3 Relative stress difference for linear incident wave

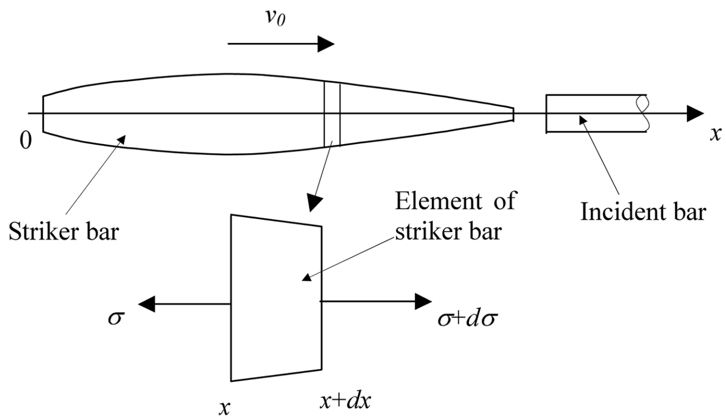

Fig. 4 Impact of an arbitrary-shape striker bar with an incident bar

3. Design of striker bar

Various methods have been used in attempting to increase the rise-time of the incident wave. Zheng *et al*. (1999) inserted a 4 mm thick carton between the striker bar and the incident bar to obtain an incident wave with prolonged rising time. Chen *et al*. (1998) used a polymer disk placed between the striker bar and the incident bar to modify the incident wave, while Ninan *et al*. (2001) used a soft material to lower the rising speed of the incident wave. Li *et al*. (2000), Lok *et al*. (2001, 2002) and Zhao *et al*. (2001) developed a tapered striker bar to generate an approximate half-sine incident loading waveform to test rock and concrete specimens, and Frew *et al*. (2002) proposed a simplified model to analyse the incident wave modified by a short and small metal cylinder (pulse shaper) placed between the cylindrical striker and the incident bar. They produced a wide variety of incident waves with extended rising durations and different shapes.

In the current work, a pseudo one-dimensional model is adopted to study the influence of the striker shape on the incident wave. Consider the stress wave generated by impact of an arbitrary, non-uniform diameter striker bar of length L on a cylindrical incident bar shown in Fig. 4. The striker bar has a variable diameter. It is assumed that the propagation of elastic wave is described by one-dimensional wave theory and that the incident bar is infinitely long. Applying Newton's second low of motion to the typical element of the striker bar, the problem can be described by the following governing differential equation, with appropriate boundary and initial conditions:

$$\begin{cases} \dfrac{\partial}{\partial x}\left(A\dfrac{\partial u}{\partial x}\right) = \dfrac{A}{c^2}\dfrac{\partial^2 u}{\partial t^2} \\ \dfrac{\partial u}{\partial x} = 0 \quad \text{at} \quad x = 0 \\ EA_1\dfrac{\partial u}{\partial x} + \rho_2 c_2 A_2 \dfrac{\partial u}{\partial t} = -\rho_2 c_2 A_2 v_0 \quad \text{at} \quad x = L \\ u = 0, \quad \dfrac{\partial u}{\partial t} = 0 \quad \text{at} \quad t = 0 \end{cases} \tag{13}$$

where u is the deformation induced displacement of the striker bar; $A = A(x)$, c and E are the cross-sectional area, longitudinal wave velocity and Young's modulus of the striker bar respectively; A_1 is the cross-sectional area of the striker bar at the impact end; c_2, ρ_2 and A_2 are the longitudinal wave velocity, density and cross-sectional area of the incident bar respectively; and v_0 is the impact speed.

The boundary condition at $x = L$ makes use of the theoretical solution of the incident wave travelling along the positive x direction in the incident bar, i.e., the stress $\sigma = -\rho c v$, in which ρ, c and v are the density, wave velocity and particle velocity respectively.

The finite difference method is used to solve Eq. (13) because the analytical solution cannot be obtained for a general shape. To do this, the length of the impact bar is divided into N equal portions by $(N + 1)$ nodes; Node "0" is at the left-hand end and node "N" the right-hand end. Using central difference approximations, the second derivative can be replaced by the following finite difference:

$$\frac{\partial}{\partial x}\left(A\frac{\partial u}{\partial x}\right) = \frac{A_{i+0.5}u_{i+1,t} - (A_{i+0.5} + A_{i-0.5})u_{i,t} + A_{i-0.5}u_{i-1,t}}{\Delta x^2} \tag{14}$$

$$\frac{\partial^2 u}{\partial t^2} = \frac{u_{i,t+\Delta t} - 2u_{i,t} + u_{i,t-\Delta t}}{\Delta t^2} \tag{15}$$

where, $u_{i,t}$ is the displacements at node i and time t; Δt and Δx are the time-step and the distance between two nodes respectively; and $A_{i-0.5}$, A_i and $A_{i+0.5}$ are the cross-sectional areas of the striker bar half-mesh size before node i, at node i and half-mesh size after node i respectively.

Substituting Eqs. (14) and (15) into the first equation of (13), and simplifying the resulting expression, leads to the displacement at internal nodes:

$$u_{i,t+\Delta t} = \frac{c_1^2\Delta t^2}{\Delta x^2 A_i}[A_{i+0.5}u_{i+1,t} - (A_{i+0.5} + A_{i-0.5})u_{i,t} + A_{i-0.5}u_{i-1,t}] + 2u_{i,t} - u_{i,t-\Delta t} \tag{16}$$

At the left end ($i = 0$), the boundary condition is expressed as:

$$\frac{u_1 - u_{-1}}{2\Delta x} = 0 \tag{17}$$

where u_{-1} is an imaginary node to the left of the computation domain. Taking $i = 0$ in Eq. (16) and substituting it into Eq. (17), after rearrangement, results in the following equation for the left end node:

$$u_{0,t+\Delta t} = \frac{c_1^2\Delta t^2}{\Delta x^2 A_0}[(A_{0.5} + A_{-0.5})u_{1,t} - (A_{0.5} + A_{-0.5})u_{0,t}] + 2u_{0,t} - u_{0,t-\Delta t} \tag{18}$$

At the right end ($i = N$), the central difference form of the boundary condition is written as:

$$EA_N\frac{u_{N+1,t} - u_{N-1,t}}{2\Delta x} + \rho_2 c_2 A_2\frac{u_{N,t+\Delta t} - u_{N,t-\Delta t}}{2\Delta t} = -\rho_2 c_2 A_2 v_0 \tag{19}$$

where u_{N+1} is an imaginary node to the right of the computation domain.

Solving equation (19) for u_{N+1} and substituting it into Eq. (16), taking $i = N$, leads to:

$$u_{N,\,t+\Delta t} = \frac{c_1^2 \Delta t^2}{\alpha A_N \Delta x^2}\Bigg[A_{N+0.5}\left(u_{N-1,\,t} + \frac{\rho_2 c_2 A_2 \Delta x}{E A_N \Delta t} u_{N,\,t-\Delta t} - \frac{2\rho_2 c_2 A_2 \Delta x}{E A_N} v_0\right) - (A_{N+0.5} + A_{N-0.5}) u_{N,\,t} + A_{N-0.5} u_{N-1,\,t}\Bigg] + \frac{2u_{N,\,t} - u_{N,\,t-\Delta t}}{\alpha} \tag{20}$$

where

$$\alpha = 1 + \frac{\rho_2 c^2 c_2 A_2 A_{N+0.5} \Delta t}{\Delta x A_N^2 E} \tag{21}$$

For known impact velocity and striker bar, the nodal displacements can be calculated at a series of time intervals according to Eqs. (16), (18) and (20). The incident stress can therefore be determined from the displacement at node N as:

$$\sigma_i(t) = -\rho_2 c_2\left(\frac{\partial u_N(t)}{\partial t} + v_0\right) \tag{22}$$

The finite difference scheme described above has been programmed and used to compute the incident stress histories for the striker shapes shown in Fig. 5. For impact speed of 10 m/s, the results for each of the striker bars are plotted in Fig. 6. Some common characteristics can be observed from Fig. 6. These are:

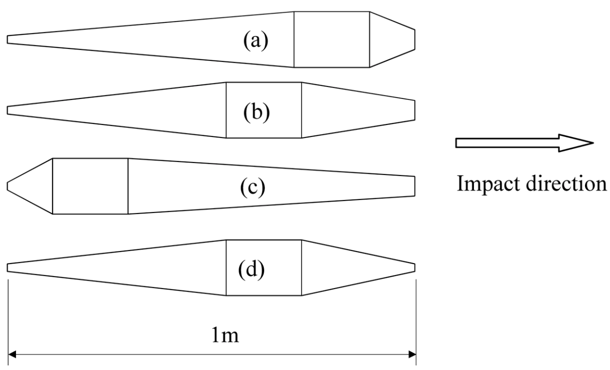

Fig. 5 Striker bars of different shapes

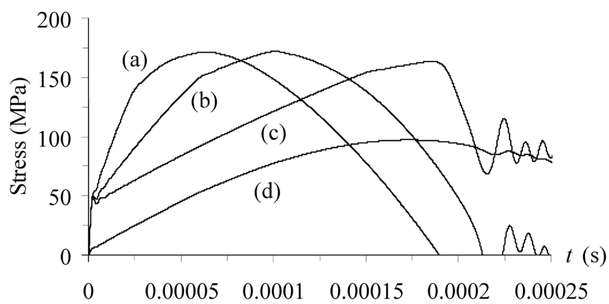

Fig. 6 Time histories of incident wave produced by different striker bars

(a) On impact, the incident stress jumps abruptly from zero to a finite value. This is related to the cross-sectional area of the striker bar at the impact end

(b) After the initial period, the incident stress increases gradually at an approximate constant rate for a certain time interval determined by the length of the linearly increasing portion of the striker bar

(c) After the peak stress, the incident stress decreases gradually. The decreasing rate is related to the length of the linearly decreasing portion of the striker bar

(d) Increasing the length of the linear portion of the striker bar at the start will increase the time duration of linearly increasing portion.

Based on these observations, two tapered striker bars were fabricated as shown in Fig. 7. Each of the bars has three linearized portions. The corresponding incident stress histories obtained from tests using these two striker bars are shown in Fig. 8 (direction of impact is from left to right). It is observed that the rise-times of the incident waves have been extended to about 100 μs and 400 μs for the short and long striker bars respectively. At these durations, stress uniformity in the specimen is guaranteed.

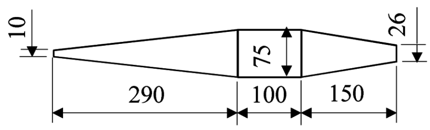

(a) Short tapered striker bar

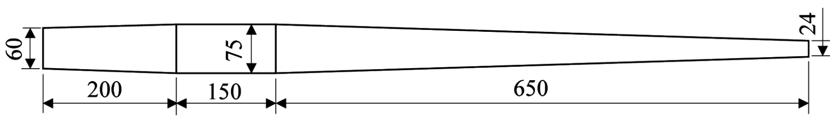

(b) Long tapered striker bar

Fig. 7 Tapered striker bars used in the investigation

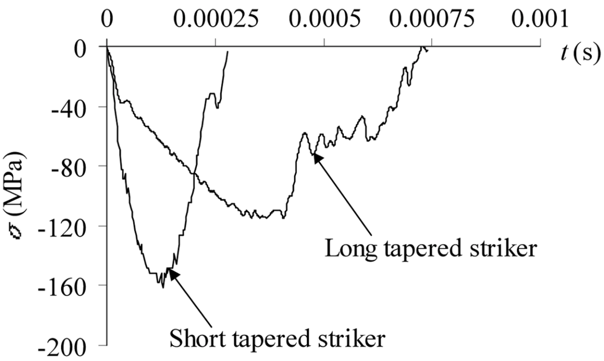

Fig. 8 Measured incident stress histories of tapered striker bars

4. Accuracy of incident stress wave

To examine the accuracy of the proposed simplified one-dimensional model using the developed finite difference algorithm, a comparison was made of the incident stress histories between the one-dimensional model, experimental data and from a finite element code (LS-DYNA).

The finite element model includes the long tapered striker bar shown in Fig. 7(b) and a 3.0 metre long incident bar. Proper contact was defined at the interface between this striker bar and the incident bar. Both the striker bar and the incident bar were divided into 25 elements in the lateral direction and the number of elements in the axial direction makes the element approximating square. As in the SHPB tests, the stress-time history was recorded on the surface element at 0.75 metres away from the interface. The length of the incident bar ensures that the complete incident stress pulse has passed the observation point before the reflected wave returns. So, the incident stress and the reflected stress were naturally separated in the stress history record.

A comparison of the incident stress histories obtained from one-dimensional model, finite element model and experimental record is shown in Fig. 9. Generally, there is good agreement on the stress histories of the three methods. The plot also indicates that three-dimensional effect, which is excluded in the simplified one-dimensional model, is not a major factor in impact tests using a shaped striker bar on a 75 mm diameter incident bar. Further, a sudden jump is evident at the initial stage of the impact in the simplified model. This is likely to be attributed to the following reasons:

- The one-dimensional model does not take account of wave dispersion. In the finite element model and experimentation, the incident stress was observed at a distance from the impact face. A sudden rise in the waveform is attenuated by dispersion in the computation and in practice.
- The assumption used in the one-dimensional wave is not reflected accurately at the initial stage for the incident bar; cross-sectional area of the striker bar is considerably smaller than that of the incident bar at the contact face. Therefore, the entire end face of the incident bar does not move simultaneously. This reduces the stiffness of the incident bar and slows down the rising rate of the incident stress.
- Imperfect alignment of the bars makes the rising rate of the incident stress slower than the theoretical condition.

However, the discrepancy between predicted and measured stress histories does not affect the applicability of this method. This is because only an approximate incident wave shape is needed

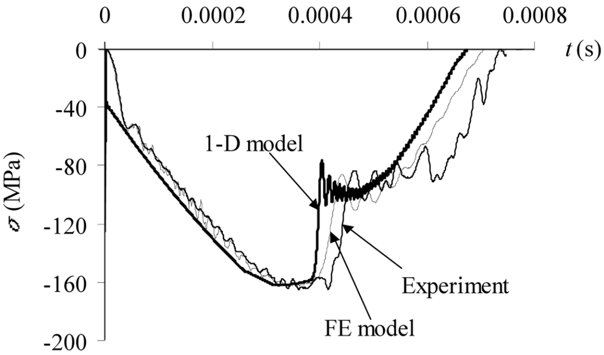

Fig. 9 Comparison of incident stress histories

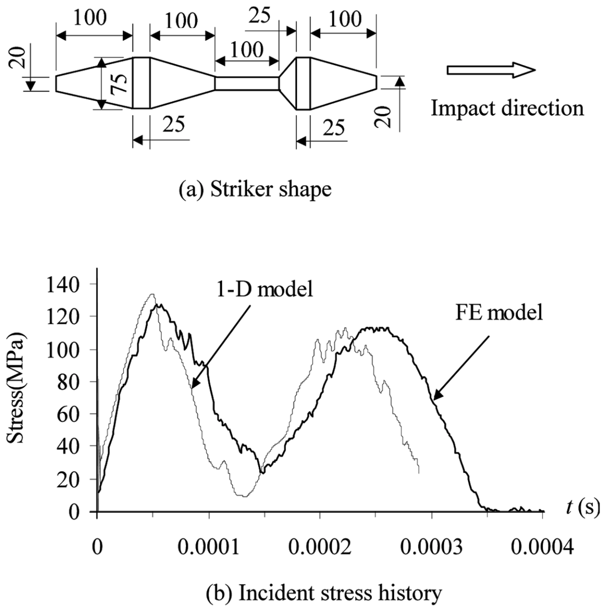

Fig. 10 Multiple shaped striker bar and incident wave

from the striker design; the actual values are measured in the test.

Clearly, the hypothesis of the striker bar design can be extended, for example, to produce repeated loading/unloading/reloading stress cycle in a split Hopkinson pressure bar test. A striker bar comprising several tapered portions along the length, each having a shape similar to the one shown in Fig. 7, could theoretically produce an incident wave containing several stress cycles from a single impact. Such an incident wave can be used for testing specimens in a stress path with unloading and reloading cycles. An example of this is shown in Fig. 10, where the predicted response derived from the proposed one-dimensional model has been confirmed by finite element analysis.

5. Application of the shaped striker bars for testing steel fibre reinforced concrete

Using the two tapered striker bars shown in Fig. 7, a number of high-strength steel fibre reinforced concrete specimens were tested. The specimens have a diameter of 70 mm and a length of 35 mm. All the specimens were obtained by coring from a large concrete block, and from which static test were also taken at the same time. The specimens have an average uniaxial static compressive strength of 90.3 MPa.

In dynamic testing, the specimens were subjected to approximately three strain rates of about 25 s^{-1}, 60 s^{-1} and 120 s^{-1}. Each strain rate comprises three specimens. Tests of specimens at 25 s^{-1} band were conducted using the long tapered striker bar since the shorter tapered striker bar was unable to perform the test at low strain rate. The other tests were conducted using the short tapered striker bar. Figs. 11-13 show typical test results using the short tapered striker bar, with measured strain histories, stress, strain and strain rate histories of the specimen and stress/strain curves.

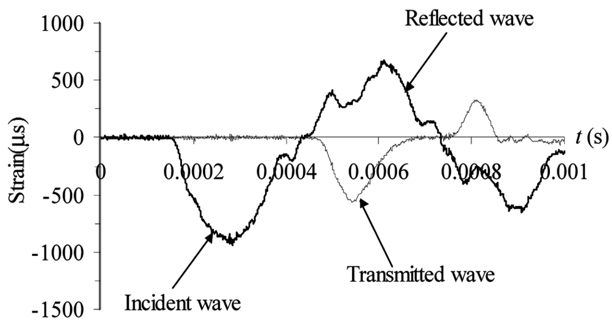

Fig. 11 Typical recorded strain histories from short tapered striker bar

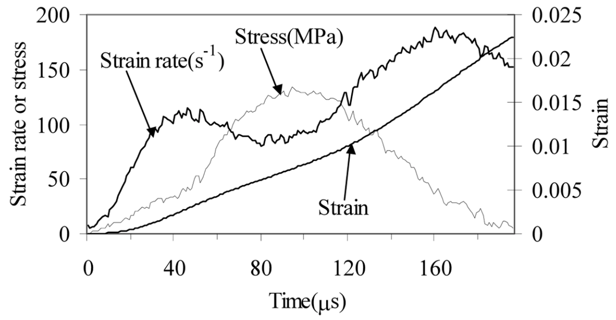

Fig. 12 Typical histories of specimen stress, strain and strain rate

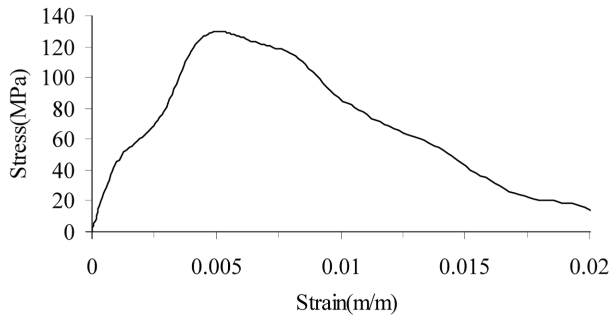

Fig. 13 Typical stress/strain curve of the specimen

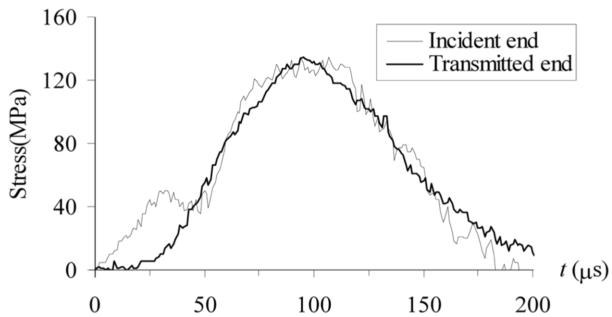

Fig. 14 Stress histories at two ends of the specimen for shorted tapered striker bar

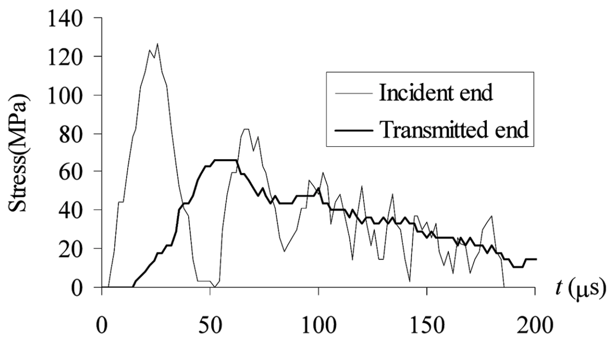

Fig. 15 Stress histories at two ends of the specimen for cylindrical striker bar

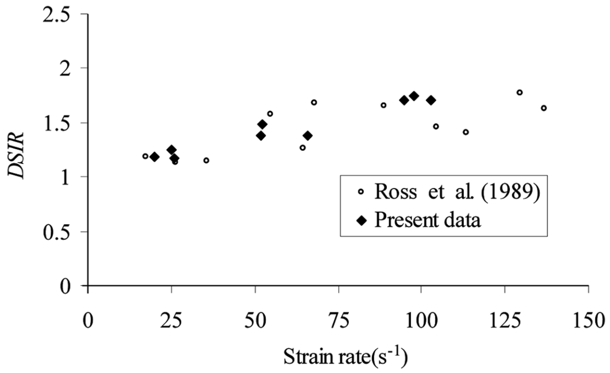

Fig. 16 Influence of strain rate on uniaxial compressive strength of SFRC

It is observed that the tapered striker bar produces smoother incident, reflected and transmitted waves than the conventional cylindrical striker bar. Using the short tapered striker bar, the histories of the stress at the ends of the specimen may be plotted as shown in Fig. 14. Clearly, a reasonably uniform stress in the specimen is achieved at about 50 μs while the specimen reaches the peak value at about 100 μs. As a comparison, similar curves are presented in Fig. 15 for an identical specimen but tested using a solid cylindrical striker bar; non-uniform stress at the ends of the specimen is observed.

The influence of strain rate on the dynamic compressive strength of SFRC is expressed by the dynamic strength increase ratio (*DSIR*), defined as:

$$DSIR = \frac{f_{cdyn}}{f_{cs}} \tag{23}$$

where f_{cdyn} and f_{cs} are dynamic and static compressive strengths respectively.

The relationship between *DSIR* and the strain rate at the peak specimen stress is plotted in Fig. 16, which also includes the experimental data below 150 s^{-1} strain rate (Ross *et al.* 1989). Closer observation indicates a slight increase in dynamic compressive strength of SFRC with strain rate. The agreement between current data and those presented by Ross *et al.* (1989) indicates that dynamic strength enhancement of SFRC (with fibre volume fraction adopted in this research) is similar to plain concrete. This is because the fibres cannot be mobilized in a dynamic environment with too many cracks in post peak response.

6. Conclusions

The most important condition to observe in testing heterogeneous materials using the SHPB is stress uniformity in the specimen. To do this, several shaped striker bars are needed to achieve the range of strain rates for testing any heterogeneous material. A single shaped striker bar is not capable of achieving the range of strain rates presented in this paper. To design striker bars, a pseudo one-dimensional model was proposed, and the finite difference method was adopted to solve the resulting mathematical problem. Details of a study on striker bar shape have been presented. The results from a comparative study confirmed the applicability of the simplified method for designing striker shapes in SHPB equipment. Two shaped striker bars were designed and fabricated. They were used to test a group of steel fibre reinforced concrete specimens over an extensive range of strain rates. Test results show that compressive strength of SFRC increases with average strain rate in the same manner as plain concrete.

References

Bertholf, L.D. and Karnes, C.H. (1975), "Two-dimensional analysis of the split – Hopkinson pressure bar system", *J. of the Mechanics and Physics of Solids*, **23**, 1-19.

Chen, W., Zhang, B. and Forrestal, M.J. (1998), "A split Hopkinson bar technique for low-impedance materials", *Experimental Mechanics*, **39**(2), 81-85.

Donze, F.V., Magnier, S.A., Daudeville, L., Maritotti, C. and Davenne, L. (1999), "Numerical study of compressive behavior of concrete at high strain rates", *J. Eng. Mech.*, **125**(10), 1154-1163.

Follansbee, P.S. and Frantz, C. (1983), "Wave propagation in the split Hopkinson pressure bar", *J. Eng. Mater. Tech.*, **105**, 61-66.

Frew, D.J., Forrestal, M.J. and Chen, W. (2002), "Pulse shaping techniques for testing brittle materials in a split Hopkinson pressure bar", *Experimental Mechanics*, **42**(1), 93-106.

Kolsky, H. (1949), "An investigation of mechanical properties of materials at very high rates of loading", *Proc. of the Physics Society of London*, Series B62, 676-700.

Li, X.B., Lok, T.S., Zhao, J. and Zhao, P.J. (2000), "Oscillation elimination in the Hopkinson bar apparatus and resultant complete dynamic stress-strain curves for rocks", *Int. J. Rock Mechanics and Mining Sciences*, **37**, 1055-1060.

Lok, T.S., Zhao, P.J., Li, X.B., Liu, D.S. and Lim, C.H. (2001), "Effect of shaped impactor on the loading waveform in a large diameter split Hopkinson pressure bar", *Proc. of 10th Int. Symp. on Int. of the Effects of Munitions with Structures*, San Diego, USA, CD-ROM (Session:Structures), DTRA(USA) & Streitkräfteamt Abteilung Infrastruktur.

Lok, T.S., Li, X., Liu, D. and Zhao, P.J. (2002), "Testing and response of large diameter brittle materials subjected to high strain rate", *J. Mat. Civil Engg*, ASCE, **14**(3), 262-269.

Meng, H. and Li, Q.M. (2003), "Correlation between the accuracy of a SHPB test and the stress uniformity based on numerical experiments", *Int. J. Impact Eng.*, **28**, 537-555.

Ninan, L., Tsai, J. and Sun, C.T. (2001), "Use of split Hopkinson pressure bar for testing off-axis composites", *Int. J. Impact Eng.*, **25**, 291-313.

Ross, C.A., Thompson, P.Y. and Tedesco, J.W. (1989), "Split Hopkinson pressure bar tests on concrete and mortar in tension and compression", *ACI Mater. J.*, **86**, 475-481.

Tedesco, J.W. and Ross, C.A. (1989), "Strain-rate dependent constitutive equations for concrete", *J. Pressure Vessel Tech.*, **120**, 398-405.

Zhao, P.J., Lok, T.S., Li, X.B. and Lim, C.H. (2001), "Behaviour of steel fibre reinforced concrete under dynamic load", *Proc. of 4th Asia-Pacific Conf. on Shock and Impact Loads on Structures*, Singapore, November 2001, 572-580.

Zheng, S., Haussler-Combe, U. and Eibl, J. (1999), "New approach to strain rate sensitivity of concrete in compression", *J. Eng. Mech.*, **125**(12), 1403-1410.